CrossMark

High-temperature formation phases and crystal structure of hot-pressed thermoelectric compounds with chalcopyrite-type structure

Atsuko Kosuga* , Yosuke Fujii, Akito Horie

Abstract In this study, we introduced the temperature-dependent formation phases and crystallographic parameters of hot-pressed silver gallium telluride $AgGaTe_2$ and copper gallium telluride $CuGaTe_2$ with chalcopyrite structure from 300 to 800 K. These two compounds are potential thermoelectric materials in the intermediate temperature range; however, the temperature-dependent formation phases and crystallographic parameters of hot-pressed samples have not yet been analyzed in detail. The crystal structure analysis based on synchrotron X-ray diffraction (SXRD) measurements clarifies that impurity phases such as Te and Ag_2Te in the $AgGaTe_2$ matrix and Te and CuTe in the $CuGaTe_2$ matrix appear at some temperature regions above 300 K. The existence of such impurity phases could be correlated with the increases of the electrical resistivity and Seebeck coefficient of the samples after multiple measurement cycles of the temperature-dependent transport properties from 300 to 800 K. The tetragonal lattice parameters a and c, tetragonal lattice volume, thermal expansion coefficients, tetragonal distortion, anion displacement parameter, and isotropic displacement parameter of the hot-pressed $AgGaTe_2$ and $CuGaTe_2$ were also analyzed. These crystallographic parameters are expected to substantially affect the thermoelectric properties of $AgGaTe_2$ and $CuGaTe_2$. Our results provide prospect of the long-term high-temperature stability and clues of the detailed analysis on the transport properties of hot-pressed $AgGaTe_2$ and $CuGaTe_2$, which should aid their development for thermoelectric applications.

Keywords Chalcopyrite; Silver gallium telluride; Copper gallium telluride; Thermoelectric; Crystal structure
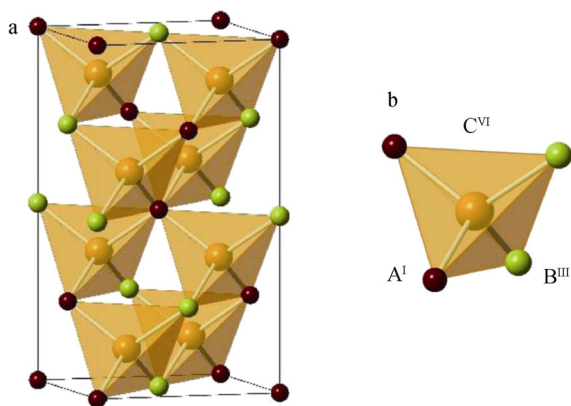
A. Kosuga*, Y. Fujii, A. Horie
Department of Physical Science, Graduate School of Science, Osaka Prefecture University, Sakai 599-8531, Japan
e-mail: a-kosuga@p.s.osakafu-u.ac.jp

A. Kosuga
JST, PRESTO, Kawaguchi, Saitama 332-0012, Japan

Y. Fujii
Department of Electronics, Mathematics and Physics, Graduate School of Engineering, Osaka Prefecture University, Sakai 599-8531, Japan

1 Introduction

The ternary compounds with chalcopyrite-type structure denoted as $A^I B^{III} C_2^{VI}$ [A = Cu or Ag (Group I elements); B = Al, Ga or In (Group III elements); and C = S, Se or Te (Group VI elements)] are currently of technological interest because they show promise for use in photovoltaics and optoelectronics [1]. These compounds crystallize in a tetragonal lattice with space group $I\bar{4}2d$ and possess four formula units per cell (Fig. 1). A^I, B^{III}, and C^{VI} atoms occupy $4a$ (0, 0, 0), $4b$ (0, 0, 1/2) and $8d$ (x, 1/4, 1/8) Wyckoff positions, respectively [2]. This structure is regarded as the stacking of two binary D^{II}–E^{VI} zinc-blended structures along the c-axis, in which one cation of a Group II element is alternately replaced by two different cations from Groups I and III elements. Each A^I and B^{III} atom is tetrahedrally coordinated to four C^{VI} atoms, while each C^{VI} atom is tetrahedrally coordinated to two A^I and B^{III} atoms (Fig. 1). The tetrahedral coordination implies that the bonding is primarily covalent with mainly sp^3 hybrid bonds, although there is some ionic character because the cations are different. This feature of the

Fig. 1 a Crystal structure of $A^IB^{III}C^{VI}$ with a chalcopyrite structure with four formula units per cell and **b** C^V-centered tetrahedron in which each C^{VI} atom being tetrahedrally coordinated to two A^I and B^{III} atoms

chalcopyrite lattice can be evaluated by two factors: tetragonal distortion, defined by $\eta = c/2a$, which is a measure of the tetragonal compression ($\eta < 1$) and tension ($\eta > 1$) along the c-axis, and the anion displacement parameter (u), which is the x-coordinate of the C^{VI} anion. The difference between A^I–C^{VI} and B^{III}–C^{VI} bond lengths shifts the u value away from the ideal cubic value of 0.25 [3].

The degree of tetragonality of compounds with chalcopyrite-type structure depends on the kinds of elements and temperature, which thereby has a considerable effect on their physical properties. In particular, the thermoelectric (TE) transport properties of these compounds has attracted considerable attention recently because they have
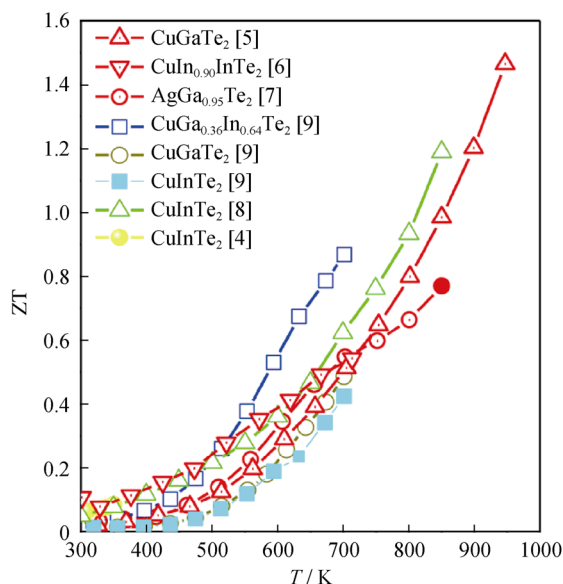
Fig. 2 Temperature dependence of dimensionless figure of merit (ZT) for representative compounds with chalcopyrite-type structure

favorable electrical properties to result in high TE performance, as shown in Fig. 2 [4–9] These properties are attributed to a good combination of the covalent and ionic bonding in the crystal structure, and are mostly controllable by changing the tetragonal parameters. Therefore, improving such properties through tuning the crystal structure of chalcopyrite-type compounds has been widely examined. For example, the band structure of this system was reported to be optimized through control of η, which is a guiding parameter to realize the highly degenerate electronic band structures that yield good electrical properties [10]. However, the temperature-dependent crystallographic parameters, including η of compounds with chalcopyrite-type structure have not been extensively studied. Furthermore, their temperature-dependent formation phases have not been studied sufficiently [11–14]. Although many attempts have been made to improve the TE properties of chalcopyrite-type compounds [15–17], they were founded on the assumption that these materials are stable over the operating temperature range, which has not been confirmed. For practical applications, TE materials should have long operating lifetimes and be maintenance-free; therefore, it is essential to consider the thermal stability of such materials to assess their reliability.

In this study, we focused on polycrystalline $AgGaTe_2$ and $CuGaTe_2$ consolidated by hot pressing, which is a typical method to prepare sintered TE materials, and their high-temperature formation phases and crystallographic parameters were examined. Hot-pressed samples are intentionally used with the purpose of evaluating the high-temperature behavior of samples intended for TE applications. This study enables understanding of the high-temperature behavior of hot-pressed $AgGaTe_2$ and $CuGaTe_2$ and provides clues to improve the high-temperature TE properties and stability of these materials for use in real TE applications.

2 Experimental

The starting materials of Ag (99.99%, shot, Rare Metallic Co., Ltd., Japan), Ga_2Te_3 (99.999%, chunk, Furuuchi Chemical Co., Ltd., Japan) and Te (99.999%, shot, Rare Metallic Co., Ltd.) were mixed to form $AgGaTe_2$ and Cu (99.99%, shot, Rare Metallic Co., Ltd.), Ga_2Te_3 (99.999%, chunk, Furuuchi Chemical Co., Ltd.) and Te (99.999%, shot, Rare Metallic Co., Ltd.) were mixed to form $CuGaTe_2$ according to the corresponding stoichiometric compositions and placed in silica vacuum tubes. The mixture was melted at 1273 K for $AgGaTe_2$ and 1173 K for $CuGaTe_2$ and kept overnight in the furnace before being quenched in water. The obtained ingot was annealed at 873 K for 72 h for $AgGaTe_2$ and 773 K for 72 h for

CuGaTe$_2$ to obtain a homogeneous ingot sample. The ingot was then crushed into a fine powder. The fine powder was sintered into a disc-like shape with a hot press using conditions reported previously [4, 5].

To characterize the crystal structural parameters and identify impurity phases of the hot-pressed samples, synchrotron X-ray diffraction (SXRD) was performed at BL02B2 beamline of the SPring-8 synchrotron radiation facility, Japan. At beamline BL02B2, a large Debye–Scherer camera and imaging plate were used for the detector. The wavelength used in this study was 0.0419712 nm refined with a CeO$_2$ standard. Each hot-pressed sample was crushed into a fine powder and then sealed in a silica capillary under vacuum. It was measured diffraction profiles of hot-pressed AgGaTe$_2$ and CuGaTe$_2$ with temperature increasing from 300 to 800 K in increments of 50 K to observe changes in crystal structural parameters and detect impurity phases with temperature. Rietveld analyses were carried out for the observed SXRD profiles using the RIETAN-FP program [18]. The average crystal structure of the main phases of AgGaTe$_2$ and CuGaTe$_2$ was refined using the tetragonal space group $I\bar{4}2d$ as a starting model. Minority phases that appeared with temperature were identified using data analysis software integrated with X-ray powder diffraction software PDXL (Rigaku, Japan). A modified split pseudo-Voigt function with Lorentz and Gauss functions for the full width at half maximum (FWHM) were applied for the profile function. The fit indicators R_{wp} and R_B were used to assess the quality of the refined structural model.

The electrical resistivity (ρ) and Seebeck coefficient (S) of the hot-pressed AgGaTe$_2$ and CuGaTe$_2$ samples were measured by the standard four-probe method using a commercially available apparatus (ZEM-3; ULVAC Technologies) at 300–800 K in helium atmosphere. To assess the high-temperature stability of the hot-pressed samples, ten cycles of temperature-dependent measurements of ρ and S were repeated.

3 Results and discussion

3.1 AgGaTe$_2$

To evaluate the temperature-dependent phase formation of hot-pressed AgGaTe$_2$, the impurity phases were identified. The chalcopyrite-type structure of AgGaTe$_2$ is the main phase at all temperatures studied (300–800 K), as shown in Fig. 3. Depending on the impurity phase(s) present, the profiles are classified into four regions: Region I (300–350 K), where only the chalcopyrite-type structure of AgGaTe$_2$ exists; Region II (400–650 K), where a small amount of Te appear as a secondary phase; Region III (at 700 K), where the Te disappears and again only the chalcopyrite-type structure of AgGaTe$_2$ exist; and Region IV (750–800 K), where small amounts of Ag$_2$Te and unidentified materials appear as impurity phases.

By taking a closer look at each region, all of the peaks are fully indexed as those of AgGaTe$_2$ with a chalcopyrite-type structure [19] in Region I, similar to the results for previously reported samples prepared by the same method [7]. In Region II, the peaks from the secondary phase of Te [20] appear at 400 K and increase in intensity up to 600 K, then their intensity decreases slightly at 650 K, corresponding to the phase contents in Fig. 3. The estimated maximum phase content of Te is ∼4.2 wt% at 600 K. SXRD patterns and results of Rietveld refinement at 350 K as a typical example of Region I and 600 K to represent Region II are shown in Fig. 4a, b. There are two possible reasons why Te appears with temperature increasing in Region II. First, small amounts of Te existing at the grain boundaries in the hot-pressed AgGaTe$_2$ would aggregate with temperature increasing. In this case, crystallite Te would be thinly dispersed through the sample or dispersed Te would be amorphous, so that crystalline Te structure is not able to be detected in SXRD pattern measured at 300 K. In an attempt to detect precipitated Te, energy-dispersive X-ray analysis was performed at room temperature on the surface of hot-pressed AgGaTe$_2$ at various observation scales, but no precipitated Te is observed. Therefore, it could be ruled out this possibility. The second possible reason why Te appears with temperature increasing in Region II is that Te was segregated from the AgGaTe$_2$ matrix with temperature rising. The occupancy of Te of AgGaTe$_2$ was refined at 600 K, resulting in a decrease of occupancy from 1.00 to 0.84 with better reliability factor (R-factor). This indicates that Te could segregate from the AgGaTe$_2$ matrix with temperature increasing in Region II.

As for Region III, the peaks from Te disappear and only the chalcopyrite-type structure of AgGaTe$_2$ is present. This result implies that Te sublimated or melted as the temperature rises. The thermogravimetry–differential thermal analysis (TG–DTA) of hot-pressed AgGaTe$_2$ reveals that there is no weight loss from the sample in this temperature range; therefore, the possibility of sublimation of Te could be disregarded. The possibility of Te melting could also be excluded because Te has a melting temperature higher than 700 K. Instead, the eutectic reaction between Te and AgGaTe$_2$ occurs at 673 K [21], meaning that Te would melt to enter the liquid phase at this ratio of Te to AgGaTe$_2$. Thereby, the peaks from Te disappear and only those of the chalcopyrite-type AgGaTe$_2$ structure are observed in Region III. In Region IV, peaks from impurity phases of Ag$_2$Te [22] and an unidentified material are
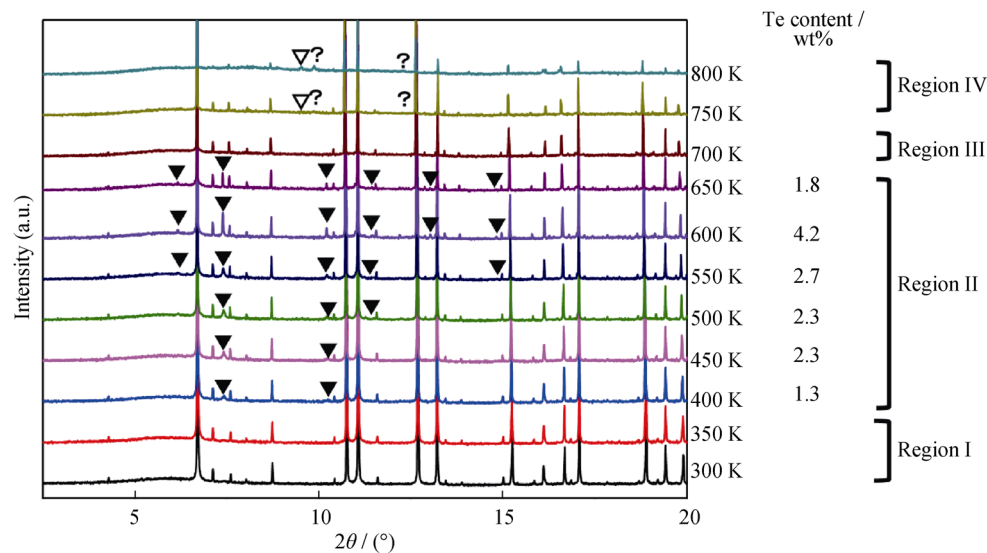
Fig. 3 SXRD data for heating process over temperature range of 300–800 K in angle range of 2.5°–20.0° (filled triangles, open triangles and question marks denoting Te, Ag_2Te, and unidentified phases, respectively; numbers I–IV referring to temperature regions used to classify profiles
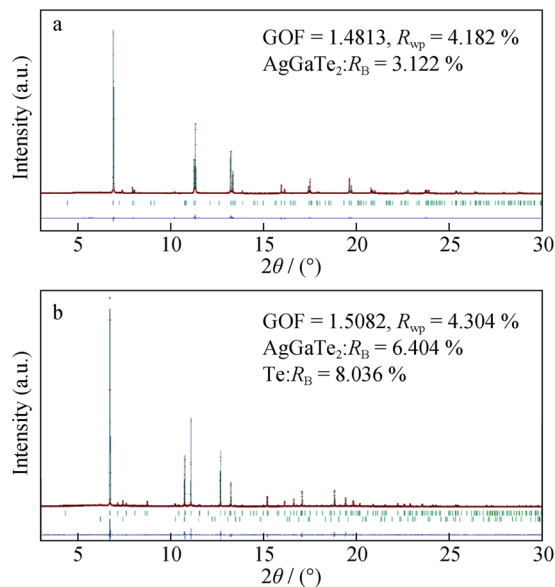

Fig. 4 SXRD patterns and results of Rietveld refinement of hot-pressed $AgGaTe_2$ at **a** 350 K and **b** 600 K (dotted and solid lines representing observed data and fitted patterns, respectively; upper and lower vertical marks indicating Bragg peaks of $AgGaTe_2$ with chalcopyrite structure and Te, respectively; blue curve at bottom being difference between observed and calculated patterns; GOF, goodness of fit; R_s and R_{wp}, reliability factors)

detected. Some of the unidentified peaks could be indexed to those of AgO [23], indicating that AgO is formed by a reaction between Ag in Ag_2Te or $AgGaTe_2$ and small amounts of oxygen in the glass capillary tube.
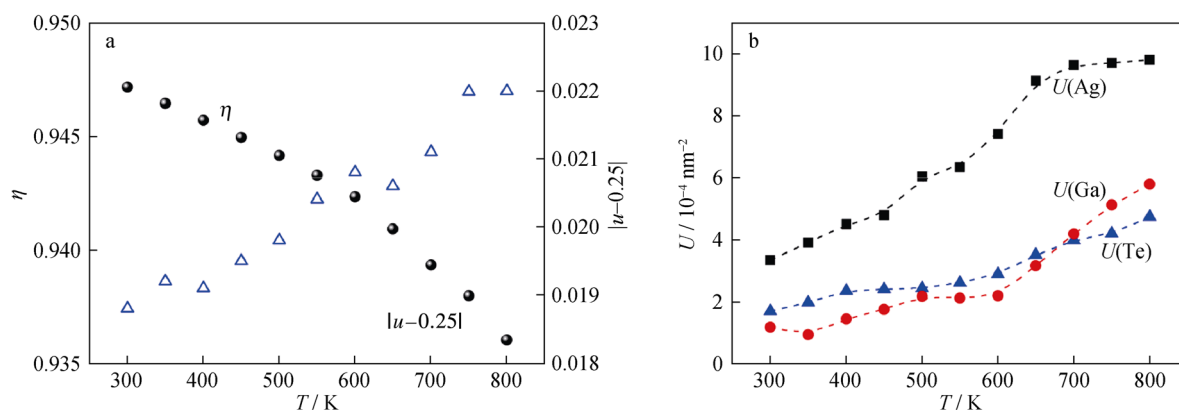
The temperature dependence of tetragonal lattice constants (a and c) and tetragonal lattice volume (V) of $AgGaTe_2$ are shown in Fig. 5. It is found that a increases and c decreases with temperature increasing, leading to

monotonic expansion of V. The calculated thermal expansion coefficients of $\alpha_a = 18.9 \times 10^{-6}$ K^{-1}, $\alpha_c = -2.48 \times 10^{-6}$ K^{-1}, and $\alpha_V = 33.8 \times 10^{-6}$ K^{-1} are slightly different from previously reported values of $\alpha_a = 13.5 \times 10^{-6}$ K^{-1}, $\alpha_c = -8.8 \times 10^{-6}$ K^{-1} [11] and $\alpha_a = 16.0 \times 10^{-6}$ K^{-1}, $\alpha_c = -6.52 \times 10^{-6}$ K^{-1} and $\alpha_V = 25.48 \times 10^{-6}$ K^{-1} [24]. Figure 6a reveals that η decreases with temperature rising, which is caused by both the decrease of c-axis and increase of a-axis with temperature elevating. The anion displacement $|u - 0.25|$ increases with temperature. These results indicate that the structure of $AgGaTe_2$ becomes more distorted with temperature increasing in terms of the tetragonal lattice and Te-centered tetrahedra. This is probably because the more ionic Ag–Te bonds have higher thermal expansion coefficients than the covalent Ga–Te bonds, and thus the anisotropy increases with temperature [1]. The isotropic displacement factor (U) for Ag, Ga and Te is illustrated in Fig. 6b. For all atoms, U increases with temperature, indicating their enhanced thermal vibration. It is notable that U of Ag is much larger than those of Ga and Te within the temperature range examined. This is probably because Ag atoms deviates considerably from their equilibrium position or Ag occupies interstitial sites in the lattice.

At high temperature (around 800 K), the hot-pressed $AgGaTe_2$ exhibits high TE performance; therefore, values of transport properties S and ρ at 800 K were plotted as a function of the number of measurement cycles (Fig. 7). The values of S and ρ were normalized to the corresponding value obtained from the first measurement. Both S and ρ rise with temperature and increases by 7% and 26%, respectively, after ten measurement cycles. It is
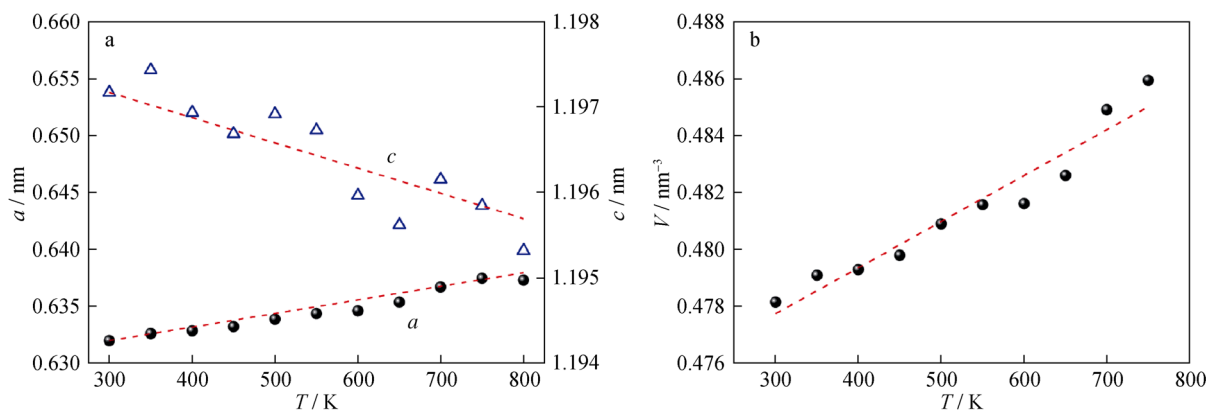
Fig. 5 Temperature dependence of **a** tetragonal lattice constants (*a* and *c*) and **b** tetragonal lattice volume (*V*) for hot-pressed AgGaTe$_2$ (dotted red lines showing fitting lines used to estimate linear thermal expansion coefficients of *a* and *b* and volume thermal expansion coefficient of *V*)

Fig. 6 Temperature dependence of **a** tetragonal distortion (η) and anion displacement $|u - 0.25|$ and **b** isotropic displacement factor (*U*) for Ag, Ga and Te
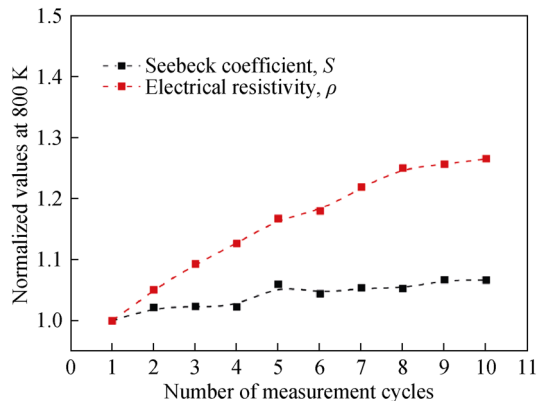
Fig. 7 Normalized values of Seebeck coefficient (*S*) and electrical resistivity (ρ) of AgGaTe$_2$ at 800 K based on value obtained in the first measurement against number of measurement cycles

presumed that these increases could originate from decrease in carrier concentration due to mainly loss of Te from the AgGaTe$_2$ matrix phase caused by repeated temperature-dependent measurement cycles from 300 to 800 K. The relative amounts of precipitations of the

impurity phases of Ag$_2$Te and Te to the matrix phase are subtle, therefore, metallic properties of such phases would not contribute to *S* and ρ of the sample.

3.2 CuGaTe$_2$

Figure 8 shows the temperature-dependent SXRD profiles for the hot-pressed CuGaTe$_2$ sample from 300 to 800 K. The profiles obtained at all the temperatures contain the chalcopyrite-type structure of CuGaTe$_2$ as the main phase. The profiles are classified into three regions according to the phase(s) present: Region I (300–450 K), where only the chalcopyrite-type structure of CuGaTe$_2$ exists; Region II (500–650 K), where small quantities of impurity phases corresponding to Te and CuTe appear; and Region III (700–800 K), where these impurity phases disappear and only the chalcopyrite-type structure of CuGaTe$_2$ is observed. The detailed changes in each region are as follows. In Region I, all of the peaks are well fitted to those of CuGaTe$_2$ with a chalcopyrite-type structure [25], confirming that the same phase is obtained as that of
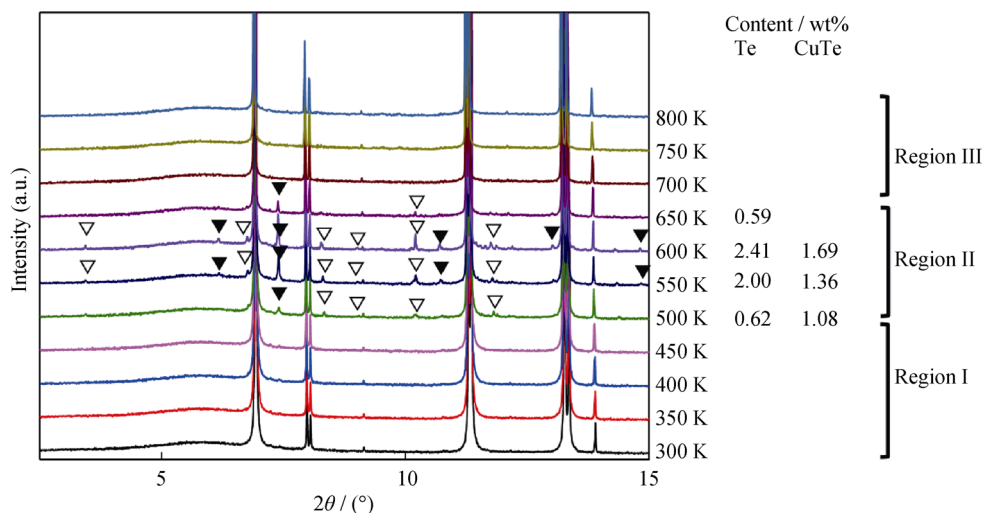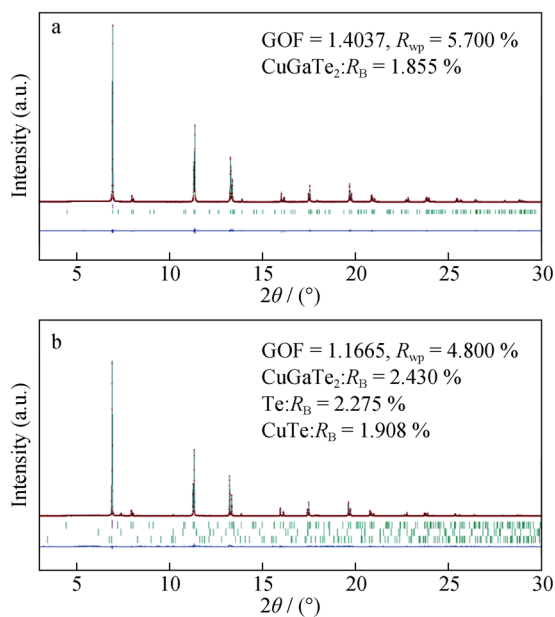
Fig. 8 SXRD data for heating process over temperature range of 300–800 K in angle range of 2.5°–15.0° (filled and open triangles denoting Te and CuTe, respectively; Numbers I–III referring to temperature regions used to classify profiles)

previously reported samples [5]. The result of Rietveld refinement at 300 K as a typical example in Region I is presented in Fig. 9a. In Region II, peaks from the impurity phases Te and CuTe appear at 500 K and increase in intensity up to 600 K, then decrease in intensity and almost disappear at 650 K, as shown by the phase content in Fig. 8. The estimated phase contents of Te and CuTe are ~ 1 wt% at 500 K and reach maximum values of 2.41 wt% and 1.69 wt%, respectively, at 600 K. The result of


Fig. 9 SXRD patterns and results of Rietveld refinement of hot-pressed $CuGaTe_2$ at **a** 300 K and **b** 600 K (dotted and solid lines representing observed data and fitted patterns, respectively; upper, middle and lower vertical marks indicating Bragg peaks of $CuGaTe_2$ with chalcopyrite structure, Te and CuTe, respectively; blue curve at bottom being difference between observed and calculated patterns)

Rietveld refinement at 600 K as a typical example in Region II is presented in Fig. 9b. Similar to the case for $AgGaTe_2$, Te and CuTe are considered to segregate from the $CuGaTe_2$ matrix with temperature increasing. In Region III, the peaks from Te and CuTe disappear and only the chalcopyrite-type structure of $CuGaTe_2$ is detected. The eutectic reaction between Te and CuTe occurs at 613 K, causing Te to melt and enter the liquid phase [26]. Thereby, the peaks of Te disappear and only those of the chalcopyrite-type $CuGaTe_2$ structure are observed in Region III.

Figure 10 shows the temperature dependence of a, c, and V of hot-pressed $CuGaTe_2$. Both a and c increase with temperature, leading to linear expansion of V. The calculated thermal expansion coefficients are $\alpha_a = 18.9 \times 10^{-6}$ K^{-1}, $\alpha_c = 8.15 \times 10^{-6}$ K^{-1}, and $\alpha_V = 34.3 \times 10^{-6}$ K^{-1} are slightly different from previously reported values of $\alpha_a = 11.7 \times 10^{-6}$ K^{-1} and $\alpha_c = 6.6 \times 10^{-6}$ K^{-1} [27]. It is found that α_c of $CuGaTe_2$ is a positive value, whereas that of $AgGaTe_2$ is negative. This result is accordance with the empirical relation proposed by Neumann [28], who stated that the thermal expansion coefficient ratio α_a/α_c is a continuous function of the axial ratio c/a, and increases with c/a decreasing. Also, there exists a critical c/a value for chalcopyrite materials, which is approximately 1.90, below which α_c becomes negative. In the current study, c/a of $AgGaTe_2$ is 1.89, which is below the critical value, while that of $CuGaTe_2$ is 1.98, above the critical value.

Figure 11a shows that η is almost independent of temperature, which is caused by the similar expansion along the a-axis (α_a) and the c-axis (α_c). Compared with the results for $AgGaTe_2$ which exhibits a positive α_a and negative α_c, the thermal expansion anisotropy of $CuGaTe_2$
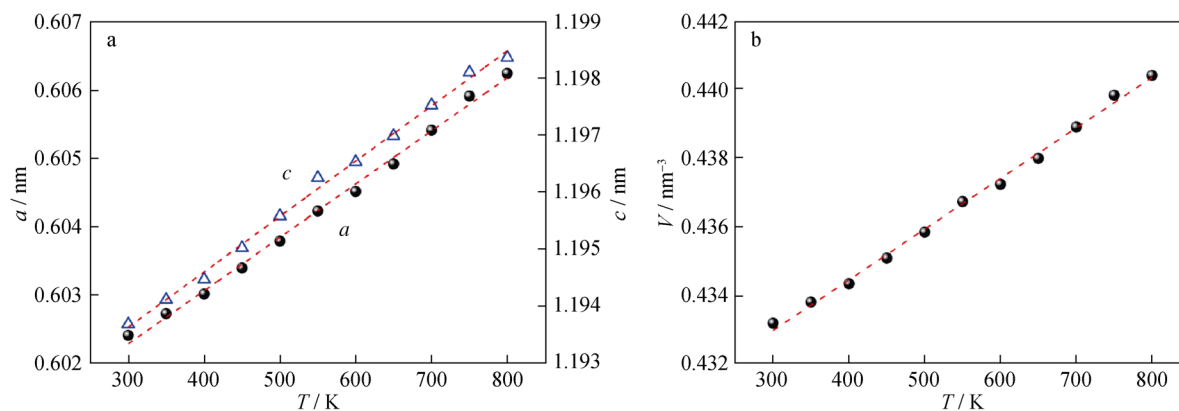
**Fig. 10** Temperature dependence of **a** tetragonal lattice constants (*a* and *c*) and **b** tetragonal lattice volume (*V*) for hot-pressed CuGaTe₂ (dotted red lines showing fitting lines used to estimate linear thermal expansion coefficients of *a* and *b* and volume thermal expansion coefficient of *V*)
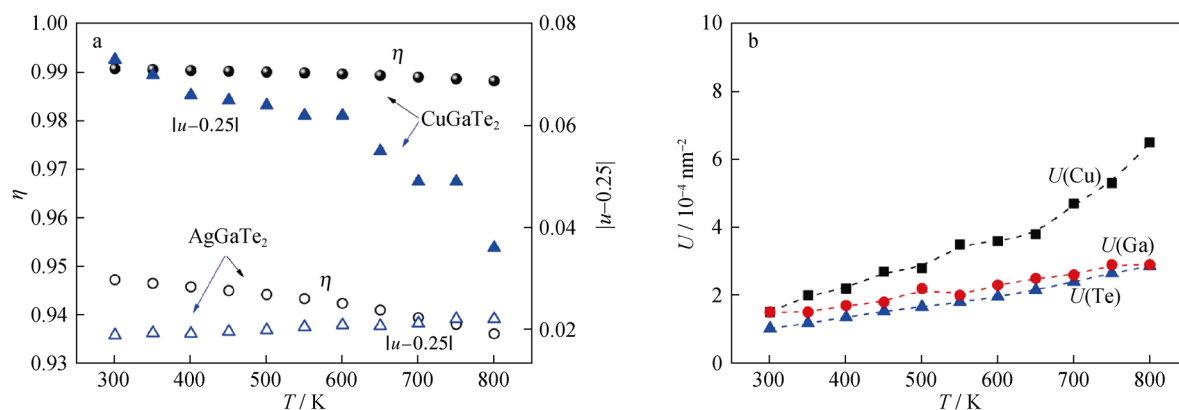
Fig. 11 Temperature dependence of **a** tetragonal distortion (η) and anion displacement $|u - 0.25|$ and **b** isotropic displacement factor (*U*) for Cu, Ga and Te

is apparently smaller than that of AgGaTe₂. The anion displacement $|u - 0.25|$ of CuGaTe₂ decreases with temperature increasing, meaning that the difference between Cu–Te and Ga–Te bond length in the CuGaTe₂ structure becomes small. This result implies that some defects at the Cu/Ga cation sites are likely to occur along with slipping out of Cu from the CuGaTe₂ matrix with elevated temperature. Considering the similarity of CuGaTe₂ with CuGaSe₂, in which formation energy of defects including Cu_{Ga} and Ga_{Cu} is estimated to be low [29], it is not surprising to arise such defects in Cu-deficient CuGaTe₂, possibly contributing to decrease in $|u - 0.25|$.

The *U* values for Cu, Ga and Te in CuGaTe₂ are shown in Fig. 11b. These values increase with temperature, indicating enhanced thermal vibration of each atom. It is notable that *U* of Cu is considerably larger than those of Ga and Te within the temperature range examined. This is probably because Cu atoms deviates substantially from their equilibrium positions or Cu occupies the interstitial sites in the lattice, as is the case for AgGaTe₂.
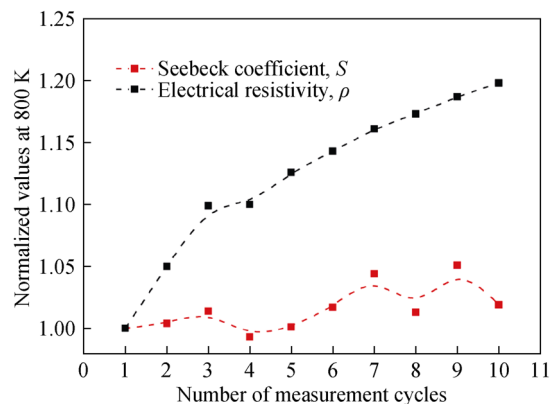
Fig. 12 Normalized values of Seebeck coefficient (*S*) and electrical resistivity (ρ) of CuGaTe₂ at 800 K based on value obtained for the first measurement against number of measurement cycles

Figure 12 shows the values of transport properties *S* and ρ for CuGaTe₂ at 800 K as a function of the number of measurement cycles. Both *S* and ρ increase with temperature, by 2% and 20%, respectively, after ten measurement cycles. These increases could partially originate from the

gradual change in ratio and/or type of impurity phases and loss of Cu and Te from the $CuGaTe_2$ matrix phase caused by repeated temperature-dependent measurements from 300 to 800 K. As is the case in $AgGaTe_2$, it is believed that these increases could originate from the decrease in carrier concentration due to mainly loss of Te from the $CuGaTe_2$ matrix phase caused by repeated temperature-dependent measurement cycles from 300 to 800 K. The relative amounts of precipitations of the impurity phases of CuTe and Te to the matrix phase are subtle, therefore, metallic properties of such phases would not contribute to S and ρ of the sample. Furthermore, the reported anomalous decrease in thermal conductivity of $CuGaTe_2$ in the intermediate temperature range [30] would be probably correlated with this formation changes observed in the current study.

It is clarified that with elevated temperature, certain amounts of impurity phases separate from both the $AgGaTe_2$ and $CuGaTe_2$ matrixes in polycrystalline samples consolidated by hot pressing. It is currently unclear whether these phenomena occur only in hot-pressed samples. Further work is needed to clarify this point, such as high-temperature SXRD analysis of powder samples of $AgGaTe_2$ and $CuGaTe_2$ before hot pressing to compare with the results of the current study. However, the results do at least suggest that the high-temperature TE properties of hot-pressed samples reported previously could be affected by changes in temperature-dependent formation phases and crystallographic parameters [5, 7–10, 15, 17]. Therefore, results in this study provide clues about the long-term high-temperature stability and transport properties of hot-pressed $AgGaTe_2$ and $CuGaTe_2$ as candidates for TE applications.

4 Conclusion

The temperature-dependent formation phases of hot-pressed $AgGaTe_2$ and $CuGaTe_2$ were investigated by collecting SXRD data over the temperature range of 300–800 K and analyzing their crystallographic parameters. Hot-pressed samples were intentionally used with the purpose of evaluating the high-temperature behavior of samples intended for TE applications. Separation of Te and Ag_2Te from the $AgGaTe_2$ matrix and Te and CuTe from the $CuGaTe_2$ matrix was observed at some temperatures between 300 and 800 K. These phenomena could cause the gradual increases of S and ρ observed over ten measurement cycles from 300 to 800 K. The U values of Ag and Cu increase with temperature and are much larger than those of the other elements in $AgGaTe_2$ and $CuGaTe_2$, respectively, within the temperature range examined, which is likely attributed to either deviation of such atoms from their equilibrium positions, or the loss of Ag or Cu atoms that occupy interstitial sites. The α_a, α_c and α_V values are slightly different from those reported previously. Analysis of $c/2a$ and u indicate that the structure of $AgGaTe_2$ becomes more distorted with temperature increasing in terms of both the tetragonal lattice and Te-centered tetrahedron. For $CuGaTe_2$, the distortion of the tetragonal lattice is almost constant with temperature. Additionally, Te moves to the equilibrium position with temperature increasing, probably caused by arising the defects of Cu/Ga cation sites. These crystallographic parameters could substantially affect the TE properties of materials; thus, the insight obtained here reveals the important parameters to evaluate the high-temperature transport properties of hot-pressed $AgGaTe_2$ and $CuGaTe_2$.

References

[1] Shay JL, Wernick JH. Ternary Chalcopyrite Semiconductors: Growth, Electronic Properties, and Applications: International Series of Monographs in the Science of the Solid State. New-york: Pergamon Press; 1975. 1.

[2] Shewchun J, Loferski J, Beaulieu R, Chapman G, Garside B. The $A_{1-y}^I B_y^I C^{III} D_{2x}^{VI} E_{2(1-x)}^{VI}$ pentenary alloy system and its application to photovoltaic solar energy conversion. J Appl Phys. 1979;50(11):6978.

[3] Jaffe J, Zunger A. Theory of the band-gap anomaly in ABC_2 chalcopyrite semiconductors. Phys Rev B. 1984;29(4):1882.

[4] Kuhn B, Kaefer W, Fess K, Friemelt K, Turner Ch, Wendl M, Bucher E. Thermoelectric properties of $CuIn_{1-x}Ga_xTe_2$ single crystals. Physica (A). 1997;162:661.

[5] Plirdpring T, Kurosaki K, Kosuga A, Day T, Firdosy S, Ravi V, Snyder GJ, Harnwunggmoung A, Sugahara T, Ohishi Y. Chalcopyrite $CuGaTe_2$: a high-efficiency bulk thermoelectric material. Adv Mater. 2012;24(27):3622.

[6] Kosuga A, Plirdpring T, Higashine R, Matsuzawa M, Kurosaki K, Yamanaka S. High-temperature thermoelectric properties of $Cu_{1-x}InTe_2$ with a chalcopyrite structure. Appl Phys Lett. 2012; 100(4):042108.

[7] Yusufu A, Kurosaki K, Kosuga A, Sugahara T, Ohishi Y, Muta H, Yamanaka S. Thermoelectric properties of $Ag_{1-x}GaTe_2$ with chalcopyrite structure. Appl Phys Lett. 2011;99(6):061902.

[8] Liu R, Xi L, Liu H, Shi X, Zhang W, Chen L. Ternary compound $CuInTe_2$: a promising thermoelectric material with diamond-like structure. Chem Commun. 2012;48(32):3818.

[9] Li Y, Meng Q, Deng Y, Zhou H, Gao Y, Li Y, Yang J, Cui J. High thermoelectric performance of solid solutions $CuGa_{1-x}In_xTe_2$ ($x = 0$–1.0). Appl Phys Lett. 2012;100(23): 231903.

[10] Zhang J, Liu R, Cheng N, Zhang Y, Yang J, Uher C, Shi X, Chen L, Zhang W. High-performance pseudocubic thermoelectric materials from non-cubic chalcopyrite compounds. Adv Mater. 2014;26(23):3848.

[11] Burger A, Ndap JO, Cui Y, Roy U, Morgan S, Chattopadhyay K, Ma X, Faris K, Thibaud S, Miles R. Preparation and thermophysical properties of AgGaTe$_2$ crystals. J Cryst Growth. 2001; 225(2):505.

[12] Guittard M, Rivet J, Mazurier A, Jaulmes S, Fourcroy P. Intermediate phases, structural determination and phase-diagram of the system Ag$_2$Te–Ga$_2$Te$_3$. Mater Res Bull. 1988;23(2):217.

[13] Wei SH, Ferreira LG, Zunger A. First-principles calculation of the order-disorder transition in chalcopyrite semiconductors. Phys Rev B. 1992;45(5):2533.

[14] Wu HJ, Dong ZJ. Phase diagram of ternary Cu–Ga–Te system and thermoelectric properties of chalcopyrite CuGaTe$_2$ materials. Acta Mater. 2016;118:331.

[15] Yang J, Chen S, Du Z, Liu X, Cui J. Lattice defects and thermoelectric properties: the case of p-type CuInTe$_2$ chalcopyrite on introduction of zinc. Dalton Trans. 2014;43(40):15228.

[16] Cheng N, Liu R, Bai S, Shi X, Chen L. Enhanced thermoelectric performance in Cd doped CuInTe$_2$ compounds. J Appl Phys. 2014;115(16):163705.

[17] Kumagai M, Kurosaki K, Ohishi Y, Muta H, Yamanaka S. Effect of ball-milling conditions on thermoelectric properties of polycrystalline CuGaTe$_2$. Mater Trans. 2014;55(8):1215.

[18] Izumi F, Momma K. Three-dimensional visualization in powder diffraction. Solid State Phenom. 2007;130:15.

[19] Avon JE, Yoodee K, Woolley JC. Solid solution, lattice parameter values, and effects of electronegativity in the (Cu$_{1-x}$A$_x$)(Ga$_{1-y}$In$_y$)(Se$_{1-z}$Te$_z$)$_2$ alloys. J Appl Phys. 1984; 55(2):524.

[20] McMurdie HF, Morris MC, Evans EH, Paretzkin B, Wong-Ng W, Ettlinger L, Hubbard CR. Standard X-ray diffraction powder patterns from the JCPDS research associateship. Powder Diffr. 1986;1(2):64.

[21] Guittard M, Rivet J, Alapini F, Chilouet A, Loireau-Lozac'h AM. Description du système ternaire Ag–Ga–Te. J Less Common Met. 1991;170(2):373.

[22] Frueh A. The use of Zone theory in problems of sulfide mineralogy. 3, polymorphism of Ag$_2$Te and Ag$_2$S. Am Miner. 1961; 46(5–6):654.

[23] Yvon K, Bezinge A, Tissot P, Fischer P. Structure and magnetic properties of tetragonal silver (I, III) oxide, AgO. J Solid State Chem. 1986;65(2):225.

[24] Kistaiah P, Venudhar Y, Sathyanarayana Murthy K, Iyengar L, Krishna Rao K. Anomalous thermal expansion of silver gallium telluride. J Appl Crystallogr. 1981;14(5):281.

[25] Masse G, Djessas K, Yarzhou L. Study of CuGa(Se, Te)$_2$ bulk materials and thin films. J Appl Phys. 1993;74(2):1376.

[26] Pashinkin A, Fedorov V. Phase equilibria in the Cu–Te system. Inorg Mater. 2003;39(6):539.

[27] Bodnar I, Orlova N. Lattice thermal expansion in CuGaT$_2$ and CuInTe$_2$ compounds over the temperature range 80 to 650 K from X-ray diffracion data. Cryst Res Technol. 1986;21(8): 1091.

[28] Neumann H. Trends in the thermal expansion coefficients of the A^{I}B^{III}C$_2^{VI}$ and A^{II}B^{IV}C$_2^V$ chalcopyrite compounds. Cryst Res Technol. 1980;15(7):849.

[29] Pohl J, Albe K. Intrinsic point defects in CuInSe$_2$ and CuGaSe$_2$ as seen via screened-exchange hybrid density functional theory. Phys Rev B. 2013;87(24):245203.

[30] Shen J, Chen Z, Lin S, Zheng L, Li W, Pei Y. Single parabolic band behavior of thermoelectric p-type CuGaTe$_2$. J Mater Chem C. 2016;4(1):209.